Nuclear Physics A452 (1986) 738-772

PROPERTIES AND CAUSES OF THE COLLECTIVE FLOW

J. CUGNON

Institut de Physique B5, Université de Liège, Sart Tilman, B-4000 Liège 1, Belgium

D. L'HÔTE

CEN Saclay, DPhN/ME, F-91191 Gif-sur-Yvette Cédex, France

Received 22 July 1985
(Revised 1 November 1985)

Abstract: The properties of the collective flow occurring in the course of nucleus-nucleus collisions are investigated within the intranuclear cascade (INC) model. Contrary to our previous work, we here use a version of the cascade where the Fermi motion of the spectators is frozen until they interact for the first time. It is shown that there is an intrinsic flow within this version of the cascade, which is essentially due to the participants. The mass dependence of the flow is studied by looking at the Ca + Ca, Nb + Nb and Au + Au systems at 400 MeV/*A*. The flow is shown to increase with the mass of the system. It decreases, for a given system, when one goes to larger energies. These features are in qualitative agreement with experiment. A quantitative comparison is attempted for the Nb + Nb case. We discuss the problems encountered with application to cascade events of a filter, which fully accounts for the efficiency of the detection system. With a crude filter, we obtain for large multiplicities a peak in the flow angle distribution. The flow angle is too small in the cascade. The uncertainty of the comparison procedure is emphasized. We turn to the causes of the flow. It is shown that in the cascade, the flow arises from the work done by the pressure built inside the compressed central region on the outer layers of the system. However, it is argued on very general grounds that the flow must be reduced by the viscosity forces. It is indicated that this effect is probably present in the cascade, but that, very likely, other off-equilibrium effects further reduce the flow. Off-equilibrium effects in general are found to be responsible for the qualitative features of the mass and energy dependence of the flow.

1. Introduction

Recent measurements using the plastic ball-wall detector at Berkeley have firmly established the existence of the so-called collective flow [1,2]). The latter can be defined as a cooperative emission of particles around a sidewards direction in large-multiplicity events. This behaviour was predicted a long time ago [3]), on the basis of hydrodynamical calculations and was interpreted as being due to the pressure built into the system. For a symmetric system, in the hydrodynamical picture, the so-called flow angle increases monotonically from 0° to 90° as the impact parameter decreases from the maximum value to 0. For an asymmetric system, the flow pattern is more complicated, especially at small impact parameters. Initially, people tried to look for the influence of the collective flow on inclusive cross sections [4]). The search for evidence turned out to be difficult, because several impact parameters are contributing to the inclusive measurements and because the clusterization in the final state of the system introduces another difficulty when comparing with experiment.

Therefore, people naturally turned to exclusive quantities, a method which was rendered possible experimentally by 4π detectors, like the plastic ball, streamer chambers and drift chambers, like Diogène. Theoretically, the emphasis is now put on the so-called global variables [5-9]). An important result was obtained recently [1]), which shows a quite different behaviour in the Ca+Ca and Nb+Nb systems at 400 MeV/A. The former does not exhibit a peak at finite angle in the so-called $dN/d\cos\theta$ distributions, whereas the latter definitely shows such a behaviour. The $dN/d\cos\theta$ distributions are constructed event by event with the help of all the momenta of the *detected* particles. In other words, the experimental quantities are subject to the acceptance of the detector, which despite the 4π geometry is not negligible [10]) and seems to be hard to define exactly.

The evidence for a cooperative effect was reinforced by a comparison with an intranuclear cascade (INC) calculation, using the Yariv-Fraenkel cascade [11,12]) and applying a filter to the calculated events to take account of the detector's efficiency. In the Nb+Nb case, the cascade was not able to reproduce the observed peak of the $dN/d\cos\theta$ distributions. At that time, it appeared natural that a cascade model does not give rise to cooperative effects, perhaps because it is a "dilute" gas model with no collectivity explicitly built therein. However, the possible rise of cooperative effects out of a cascade dynamics had already been mentioned several years ago [13-15]). Pursuing this direction, we calculated last year the collective flow for the Ca+Ca and Nb+Nb systems from the cascade model developed at Liège [16]). We showed that the cascade contains intrinsically a flow pattern. In view of the complexity of the filtering procedure, supposed to simulate the acceptance of the apparatus, we were not able to predict the flow angle precisely. But within the uncertainty (about 5°), our calculation agreed with experiment (however, see the discussion in sect. 5). We also showed that the Ca+Ca displays an intrinsic flow, whose existence is hidden in the $dN/d\cos\theta$ distribution because of the event-by-event fluctuations.

Unfortunately, we used an unfrozen version of our cascade code, where the spectators are not confined. As observed by Stöcker [17]) and discussed in ref. [18]), this undue motion of the spectators spuriously increases the flow. This is the reason why we investigate here the collective flow with a frozen version of the cascade, where the Fermi motion of the spectators is frozen until they interact for the first time. More specifically, we address the following questions:

(i) Is there a flow inside the INC?

(ii) What is the energy and mass dependence of the flow?

(iii) Is the flow inside the INC sufficient to explain the experimental data?

(iv) What is causing the flow, inside the INC and in general?

The answer to the third question implies a step further compared to the other questions, since it involves the efficiency of the apparatus and the way it can be taken care of inside a cascade model.

In sect. 2, we briefly describe the model. In sect. 3 we comment on the differences between the frozen and unfrozen versions. In sect. 4, we present our numerical

results in detail. We concentrate especially on the mass and energy dependence of the flow. We also analyze the flow due to all the nucleons and the flow due to the participants only. We show that the flow angle for the latter is larger than for the whole system, but that the corresponding ellipsoid is more spherical. Sect. 5 is devoted to the comparison with experiment. We stress that the experimental filter introduced by the apparatus is not directly applicable to INC events, essentially because of the clusterization, which is not directly predicted by the INC. We therefore apply here a "standard" filter, which accounts for the gross features of the efficiency. We show the arbitrariness brought in by our procedure. The conclusions of this analysis are that, in all likelihood, the INC flow is too small compared to experiment. In sect. 6, we investigate on very general grounds the possible causes of the flow. We show that the flow is generated by the work done by the pressure forces on the outer fringes of the system. The friction forces and the off-equilibrium effects in general reduce the flow. We indicate that the qualitative mass and energy dependence observed both experimentally and within the INC, are due to these two effects. Finally, sect. 7 contains our conclusion and a discussion on the relation between our INC model and others, and on the comparison with hydrodynamics.

2. The model

The basic INC model that we have used previously is described in refs. [13,19]). Let us recall that within this version the Δ's have a finite lifetime and the pions interact with the nucleons. A point under special focus in this paper is the treatment of the spectators. In ref. [16]), the spectators are given initially a velocity due to the combination of the nucleus motion and of their Fermi motion, and are subsequently left free to move with this velocity. As noticed in refs. [13,20]) and criticized in refs. [17,18,20]), this introduces a spurious expansion of the nucleus even in the absence of perturbations. This is not a crucial problem at high energy, but at 400 MeV/A the situation is changed due to the larger interaction times. Therefore, we improve our model by "freezing" the spectators until they interact, following an idea introduced in ref. [20]). This "freezing" should be considered as a convenient means of coping with the binding energy and Fermi motion in a classical transport theory. This problem is still unresolved and lies beyond the scope of this paper.

Specifically, we record the Fermi motion velocity of the nucleons, but the latter are given the nucleus velocity before they interact. Once they are involved in a collision, they are given back their original momentum. A little indeterminacy arises in the examination of the criterion to make a collision. The latter can be written as

$$\pi r_{12}^2 \leqslant \sigma_{\mathrm{tot}}(s)\,, \tag{2.1}$$

where r_{12} is the minimum relative distance between nucleons 1 and 2, and where $\sigma_{\mathrm{tot}}(s)$ is the total cross section at the squared c.m. energy s. Should s be taken as coming from the "frozen" kinematics or from the original momenta (coming from

the nucleus plus Fermi motion)? We have adopted here the second choice, to be consistent with the energy-momentum content of the collision which is about to happen. Furthermore, the freezing of the Fermi motion should be considered as a trick to keep the nuclei confined and should not constitute a modification of the momentum content.

At the end of the collision process, signalled by the absence of nucleon–nucleon collisions, the spectators are given back their original Fermi motion. This is in keeping with the observed fragmentation of the spectators part [21-23]). We want to mention a difference between the "freezing" of ref. [20]) and ours. In ref. [20]), the moment at which the collisions occur is determined with the unfrozen kinematics, although the nucleons are proceeding along trajectories determined by the frozen kinematics. As a result, the quantity r_{12} in eq. (2.1) is not the minimum distance in this kinematics. This has no importance except for very central collisions (see sect. 3).

In this paper, we are primarily concerned with flow properties, carried by the sphericity tensor

$$Q_{ij} = \sum_{\nu} \gamma(p^{\nu}) p_i^{\nu} p_j^{\nu} , \tag{2.2}$$

where p_i^{ν} is the ith cartesian coordinate of the momentum of the νth ejectile in the c.m. system of the nuclei. The weight factor is chosen throughout this paper as $(2m_{\nu})^{-1}$, (m_{ν} being the ejectile mass), which makes the tensor coalescence-invariant [9]). The eigenvalues of the tensor are denoted by λ_i ($\lambda_1 \geqslant \lambda_2 \geqslant \lambda_3$) and the unit eigenvectors by e_i. We also introduce the first and second aspect ratios:

$$q_1 = \lambda_1/\lambda_3 , \qquad q_2 = \lambda_2/\lambda_3 . \tag{2.3}$$

The flow angle θ is conventionally defined as the angle between the largest axis and the beam axis.

3. Comparison between frozen and unfrozen versions

3.1. FLOW PROPERTIES

We concentrate our attention first on the distribution of the flow angle for an intermediate impact parameter in Nb+Nb collisions at 400 MeV/A (fig. 1, right side). The importance of intermediate impact parameters has been stressed in refs. [16,27]). The well-defined peak obtained with unfrozen spectators has shifted to smaller angles and has broadened a little bit. But the presence of a peak *clearly survives.* For central collisions (fig. 1, left side), the flow angle increases on the average when going from the unfrozen to the frozen version. We want to stress, however, the extreme sensitivity of the results, for $b = 0$, on the way the freezing is performed. In fig. 1, the dotted line represents the results with a freezing method

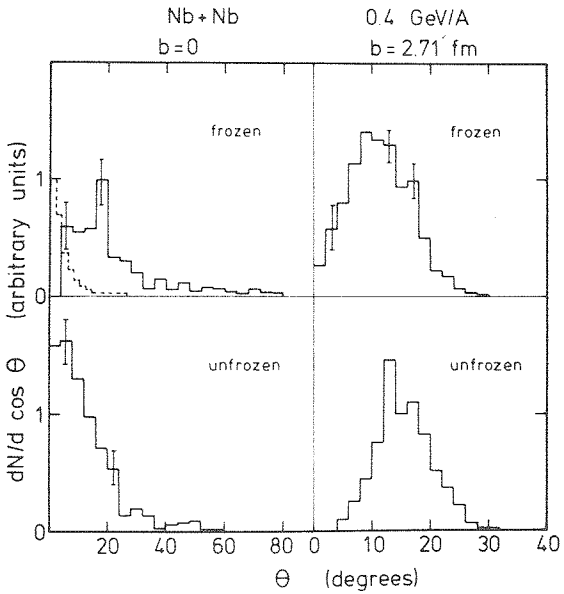

Fig. 1. Comparison between the frozen and unfrozen versions of our cascade calculations, for two impact parameters of the Nb+Nb collisions at 0.4 GeV/A. The calculated quantity is the $dN/d\cos\theta$ (see sect. 2) distribution for all the nucleons, normalized in the same way for both versions. The dotted line corresponds to a method of freezing close to the one used in ref. [20]). The histogram is normalized on the same maximum as the full-line histogram in the same box. See text for details. The error bars give the typical uncertainty of the calculations. Note the different horizontal scales for the left and right parts of the figure.

close to the one used in ref. [20])*. This sensitivity can be understood in view of the near isotropy of the sphericity tensor for $b=0$ (see fig. 10) and the geometrical aspects of the freezing (see fig. 3). For the other impact parameters shown here, the results are *not* sensitive to the freezing. This is also confirmed by other calculations [45]). The freezing used here being done in a more consistent way, we keep on with this method. Furthermore, the central collisions have little practical importance indeed (see fig. 14).

Fig. 2 shows the comparison between the two versions for two important distributions, that we will discuss extensively later on, namely the flow angle calculated after applying the standard filter [16]) in order to simulate on a simple manner the acceptance of the plastic ball-wall detector and the flow angle corresponding to the participants alone. Here and throughout this paper, the participants are defined as those nucleons which have undergone a momentum transfer of more than p_F, the Fermi momentum, taken equal to 270 MeV/c. The same observations are in order. The peak in the $dN/d\cos\theta$ distribution shifts to smaller angles, but the peak is nevertheless still visible.

* The difference is that for technical reasons the freezing has been disregarded in the pion-nucleon collisions.

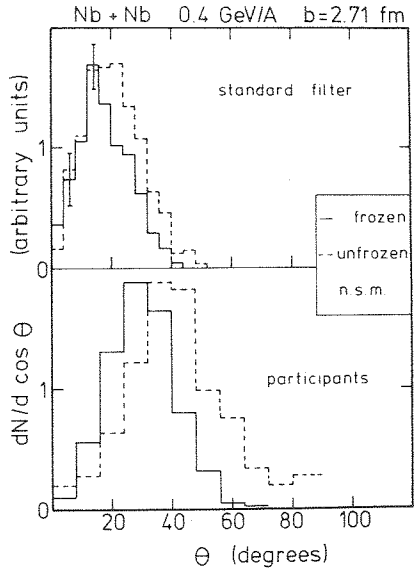

Fig. 2. Same as fig. 1, but the calculated quantities here are the $dN/d\cos\theta$ distributions for the participants only (lower part) and for the filtered events. See text for details. The distributions are normalized to the same maximum.

3.2. CASCADE FEATURES

We postpone to sect. 6 the important question of what is causing the flow. We just try here to examine what is changed in the machinery of the INC model when the spectators are frozen. As shown in fig. 3, the spurious expansion of the nuclei has two consequences. When provided with their Fermi motion, nucleons like B

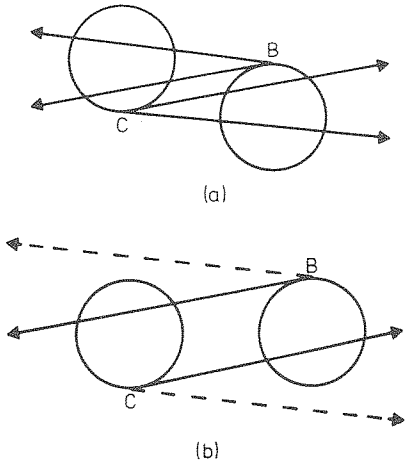

Fig. 3. Illustration of the effects induced by the unfrozen version of the cascade. See text.

and C do not align with the beam axis but have a transverse component. They thus embrace a larger part of the target than they would do without Fermi motion. This has a tendency to enlarge the participant zone, or at least to increase the number of participants. On the other hand, with the target expanding, they "see" a more dilute system. To dare a picture, they probably see a smaller optical depth. For central collisions, however, the situation is somewhat reversed. Nucleons B and C miss the partner nucleus half of the time. Therefore, it is expected that, with unfrozen spectators, the interaction zone is populated too much for large impact parameters and not enough for rather central collisions. At least this interpretation is consistent with fig. 4, which shows the number of participants M_p, as a function of impact parameter for the two versions.

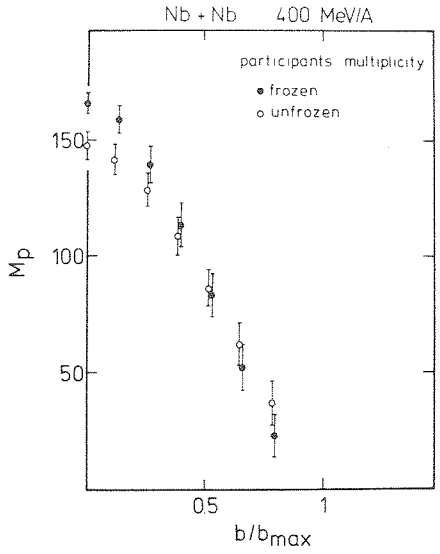

Fig. 4. Multiplicity of the participants as a function of the impact parameter for the Nb + Nb system at 0.4 GeV/A, as calculated in the frozen and unfrozen versions. The error bars give the standard deviation of the event-to-event fluctuations.

Fig. 3 and the above discussion also help us to understand the sensitivity to the method of freezing for $b = 0$. Using different methods may or may not fulfill (2.1). For a nucleon like B of fig. 3a, this is not crucial, since it has plenty of chances to interact. However, a nucleon like B of fig. 3b may escape from the interaction zone if it misses a collision. From purely geometrical considerations (see fig. 3), one can guess that the freezing is important for impact parameters $b/2R \leqslant p_F/2p_0$, where p_0 is the incident momentum. In the Nb + Nb case, this gives $b \leqslant 1$ fm.

Fig. 5 gives a comparison between the two versions at the level of various physical quantities. As for the density, there is a substantially larger compression in the

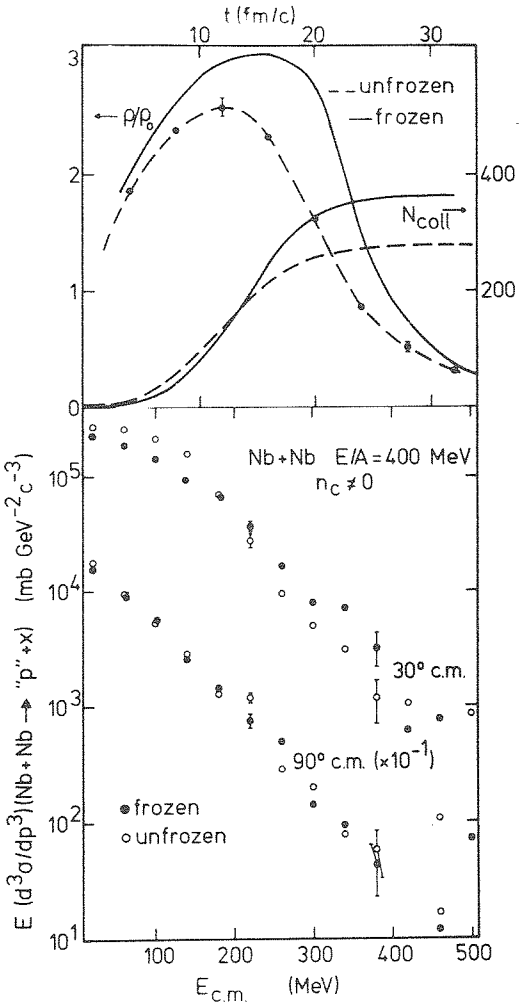

Fig. 5. Comparison between frozen and unfrozen versions of the cascade. The upper part of the figure gives the time variation of the baryon density at the location of the total centre of mass and of the number of baryon-baryon collisions. It refers to a $b = 2.71$ fm collision between two Nb nuclei at 400 MeV/A. The lower part gives the invariant-charge ("p") production cross sections at two c.m. angles. This quantity is calculated from all the nucleons which suffered at least one collision.

frozen version, which results from a higher density in the interaction region. Surprisingly, this is accompanied by a faster decompression. The number of pions (not shown) is not very much changing when going from one version to the other.

Another interesting feature is contained in fig. 5, which compares the number of baryon-baryon collisions occurring in the two versions. When the nucleons are frozen, the number of collisions is smaller at early collision times and increases later on. This seems to be correlated with a longer compression stage. Note, however,

that the increase of the number of collisions is counterbalanced by the fact that late collisions are much softer than early ones [25]).

The lower part of fig. 5 gives the comparison between the frozen and unfrozen versions as far as the inclusive cross sections are concerned. At 90° c.m. there is no practical difference between the two versions, but at 30° c.m. the cross section is larger at low energy and smaller at high energy in the unfrozen version. We think that this is probably due to the reduction of the spectator number and the increase of the number of collisions. This figure clearly shows the sensitivity of the inclusive cross sections to some features of the cascade dynamics. It then becomes highly desirable to have these experimental data available.

4. Mass and energy dependence of the flow

4.1. MASS DEPENDENCE

4.1.1. All the nucleons. To study this important question (see sect. 6), we have investigated three systems at 400 MeV/A, namely Ca+Ca, Nb+Nb and Au+Au. We first present the results of the calculation for the $dN/d\cos\theta$ distribution [26]) for several impact parameters in fig. 6. For $b=0$ collisions, we calculated 160, 100 and 28 events for the Ca+Ca, Nb+Nb and Au+Au systems, respectively. For the three next impact parameters, these numbers become 640, 400 and 112, respectively. For larger impact parameters, the statistics is the same as for $b=0$. This statistic is sufficient to guarantee accurate estimates of average values and dispersions, as explained in appendix A. The histograms refer to what we have called the *intrinsic* flow for all the nucleons [6]). By intrinsic, we mean the flow tensor calculated without any filter of any sort. A systematic pattern clearly arises from this figure. The maximum of the $dN/d\cos\theta$ distribution is practically at 0° for the Ca+Ca case, and at non-zero angles for the other two systems. The angle at which it occurs decreases for increasing impact parameter. For a given impact parameter (more precisely, for a given b/b_{max} ratio), the peak is located at a larger angle for the Au+Au case. A systematic although not spectacular feature is the narrower distribution for the Au+Au compared to the Nb+Nb system, except for $b=0$. It seems that for $b=0$, for both the Nb+Nb and Au+Au systems, we obtain a broad peak at finite angle with this frozen version, contrary to what we obtained previously with unfrozen spectators [see fig. 1 and ref. [16])].

More insight can be gained if one looks to the projection of the extremity of a unit vector attached to the centre of the ellipsoid and pointing in the direction of the largest axis (i.e. in the direction of e_1) on a plane perpendicular to the beam axis (fig. 7). Such a plot reveals the azimuthal orientation of the ellipsoid, a degree of freedom which is integrated out in the $dN/d\cos\theta$ plot. To be precise, if we define $\rho=\sin\theta$ (the distance from the centre of the square in fig. 7), the plots in

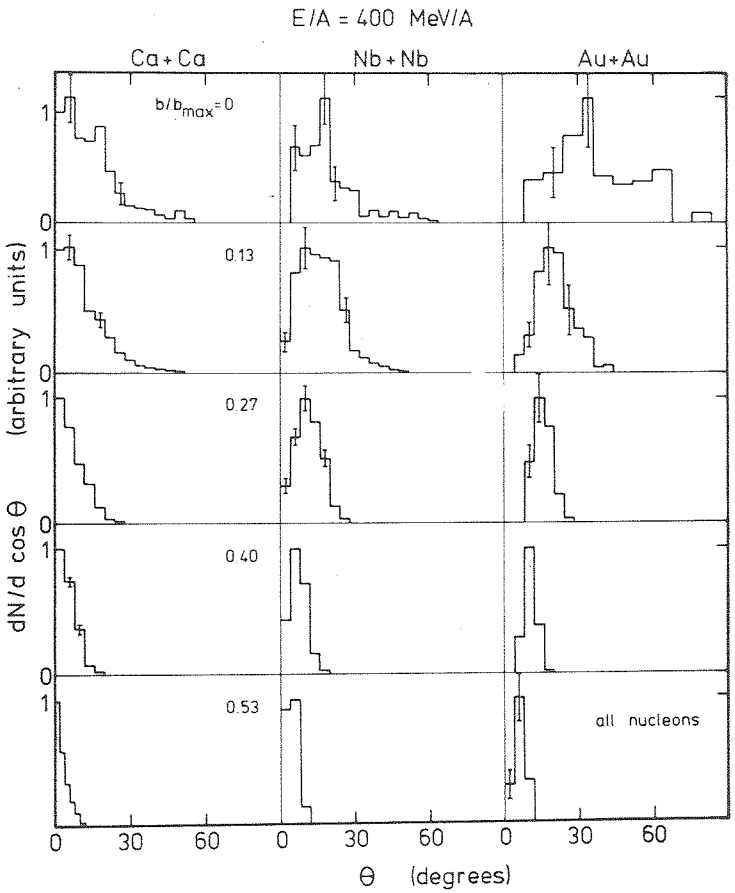

Fig. 6. $dN/d\cos\theta$ distributions for several impact parameters and for three different systems at 400 MeV/A as calculated in our INC model. The distributions are normalized on the same maximum. They correspond to all the nucleons. The error bars give the typical uncertainty of the calculation.

fig. 7 represent the distribution

$$\frac{d^2N}{\rho\, d\rho\, d\varphi} = \frac{d^2N}{\cos\theta\, d(\cos\theta)\, d\varphi}. \tag{4.1}$$

The $dN/d\cos\theta$ distribution can be obtained from the latter by

$$\frac{dN}{d(\cos\theta)} = \sqrt{1-\rho^2}\int d\varphi \left(\frac{d^2N}{\rho\, d\rho\, d\varphi}\right), \tag{4.2}$$

i.e. by simply summing over φ, for not too large values of ρ.

For central Ca+Ca collisions, the vector e_1 points on the average in the forward direction, which corresponds roughly to having the barycenter of all the points in the first square of fig. 7 at the center of this square. For intermediate impact parameters like $b = 2.04$ fm, the vector e_1 points on the average at some finite θ along the impact parameter side ($\varphi = 0$). To obtain the $dN/d\cos\theta$ plot, one has

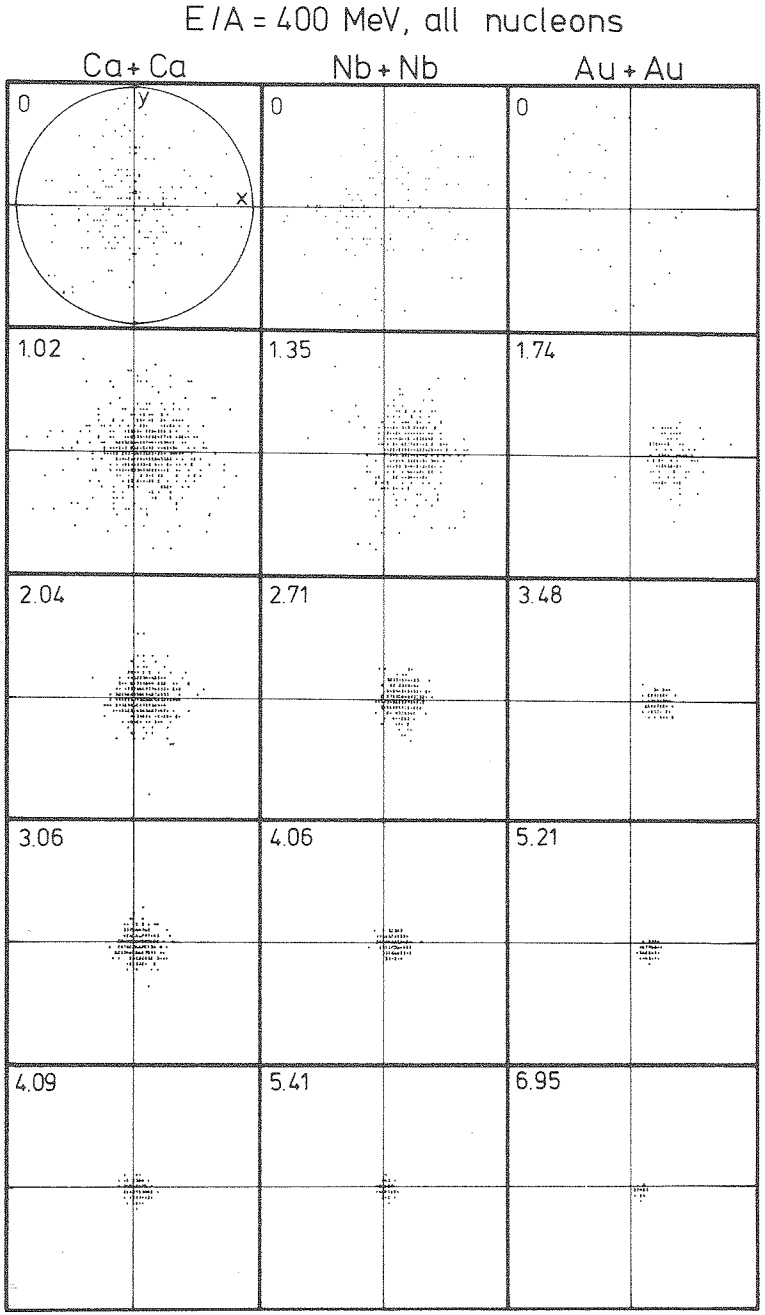

Fig. 7. Projection of the extremity of a unit vector aligned with the largest axis e_1 of the sphericity ellipsoid (for all the nucleons) on a plane perpendicular to the beam axis (the so-called meridian orthographic projection). The projection of the beam axis is the point at the center of the cross in each of the squares. The impact parameter axis is the right part of the x-axis. A single point corresponds to a single event. Different symbols not recognizable on the figure correspond to several events. The number of events for a given impact parameter is given in subsection 4.1.1. Note that, for a given system, the total number of events is the same for all the $b \neq 0$ impact parameters.

to integrate over φ according to eq. (4.2). It is suggestive from fig. 7 that because of the large dispersion of the direction of the vector e_1 this operation will give a maximum at $\theta = 0$ for the $dN/d\cos\theta$ distribution. For Nb+Nb, and even more for Au+Au, the vector e_1 points at a larger angle and the dispersion is smaller. Then, the integration over φ is not able to wash out the orientation of e_1 at finite θ. The mathematical condition for the survival of a peak is derived in appendix B for the case of a distribution (4.1) of gaussian type. As already explained in refs. [15,16,26]), the fluctuations in e_1 are related to the number of the nucleons participating in the sphericity tensor: the larger this number is, the smaller the fluctuations are. This feature was first pointed out by Danielewicz and Gyulassy [26]). For some limiting one-body distribution functions, the fluctuations should follow a simple $1/\sqrt{N}$ law (where N is the number of particles). Of course, this law is only qualitatively fulfilled here, because the one-body distribution function is not a simple function like e.g. a boltzmannian. For more detail, see refs. [26,27]).

4.1.2. The participants. The properties of the sphericity tensor described in the previous subsection result from the superposition of two ellipsoids, one for the participants and one for the spectators. These two ellipsoids have different properties. The second one is rather elongated, points towards the forward direction, and has very small fluctuations, the latter being the result of the Fermi motion only. The ellipsoid of the participants is much less elongated, points towards larger angles and carries the largest part of the fluctuations, as shown in fig. 8. An interesting feature is the appearance of hydrodynamical behaviour in the case of central ($b = 0$) Au+Au collisions: the participant ellipsoid points toward 90° c.m. and has an oblate shape (for half of the time) as revealed by fig. 9. The latter shows the distribution of the eccentricity [9])

$$\varepsilon = \frac{\lambda_s - \frac{1}{2}(\lambda_2 + \lambda_r)}{\lambda_1 + \lambda_2 + \lambda_3}. \tag{4.3}$$

In this equation, λ_s is the eigenvalue linked to the axis of quasi-symmetry. It is λ_1 if $(\lambda_1 - \lambda_2) > (\lambda_2 - \lambda_3)$ or λ_3 if $(\lambda_1 - \lambda_2) < (\lambda_2 - \lambda_3)$. λ_r is the remaining eigenvalue. The eccentricity ε is positive ($0 < \varepsilon < 1$) for prolate shapes and negative for oblate shapes ($-0.5 < \varepsilon < 0$). It carries information which is somewhat equivalent to q_2, if q_1 is known. Note that the distribution $f(\varepsilon) = dN/d\varepsilon$ of fig. 9 is not jacobian-free [26]).

The tendency to hydrodynamical behaviour is already present in Nb+Nb. Note that this kind of behaviour is less marked with the frozen-spectators version than it was with the unfrozen one [16]). The overall pattern is also corroborated by fig. 10, which shows the shape (actually the aspect ratio q_1 (eq. (2.3)) for the various ellipsoids and for the various systems under consideration.

4.2. ENERGY DEPENDENCE

To show this dependence, we have calculated the flow properties for Nb+Nb at 650 MeV/A and for Au+Au at 800 MeV/A. The results are displayed in fig. 11 for

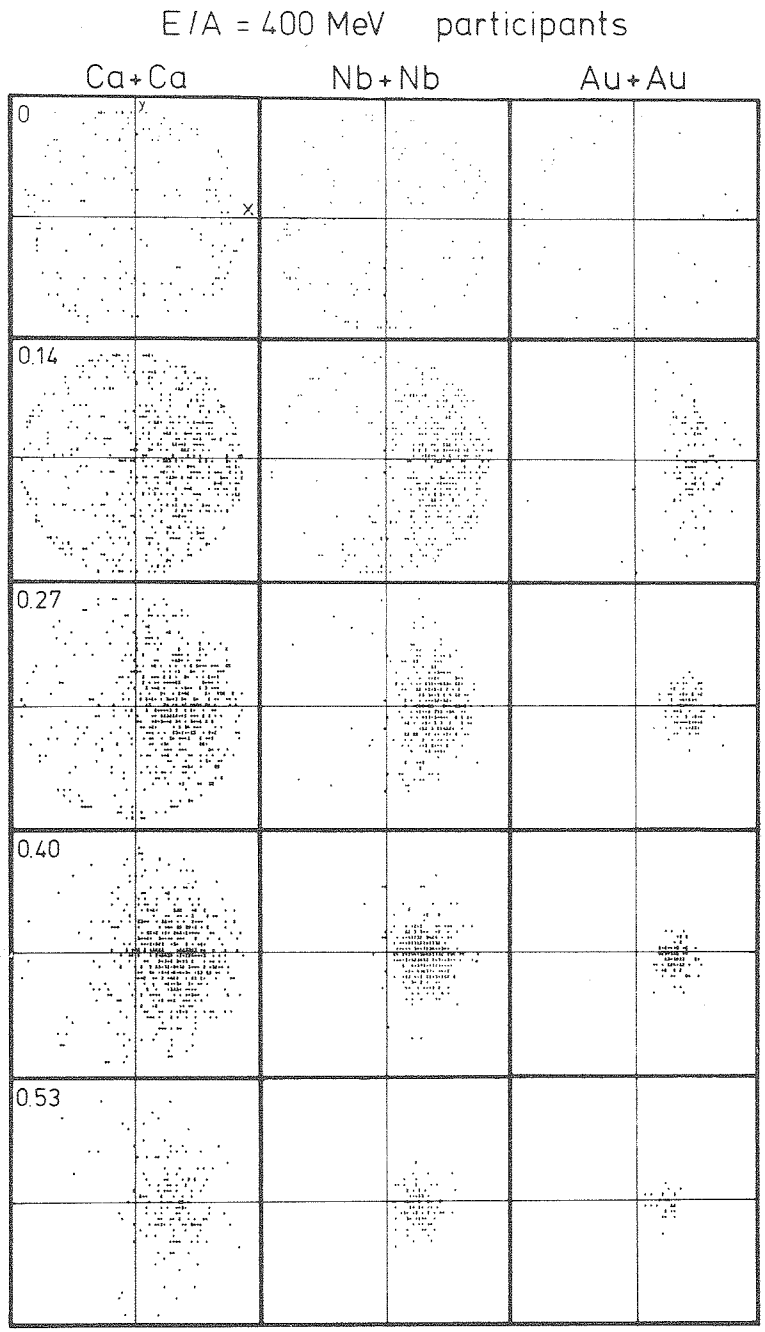

Fig. 8. Same as fig. 7, but for the participants only.

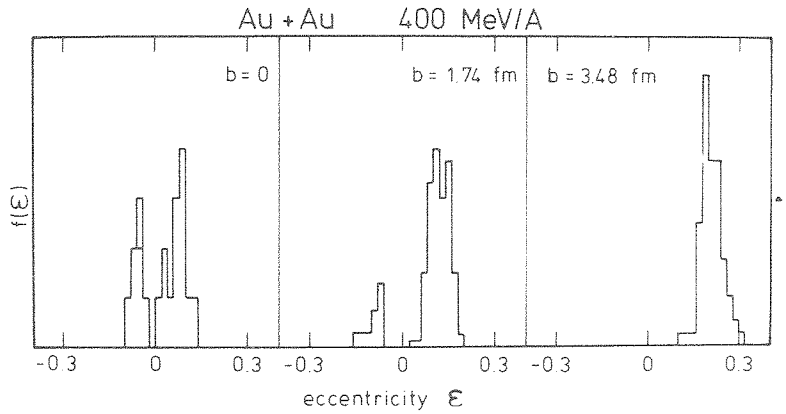

Fig. 9. Calculated distribution of the eccentricity (see eq. (4.3)) for Au+Au events at 400 MeV/A.

the smallest impact parameters and compared to the 400 MeV/A case. For Au+Au at 800 MeV/A, and for every impact parameter shown, the peak has moved towards small angles. For the Nb+Nb case at 650 MeV/A, the situation is less marked. For $b=0$, the distribution has substantially shifted to smaller angles. For the other impact parameters, the peak has not really moved but there is a tendency for the ellipsoid to point towards smaller angles as well. We will come back to this point in sect. 6, but we mention that this tendency is observed experimentally, on the filtered events, of course.

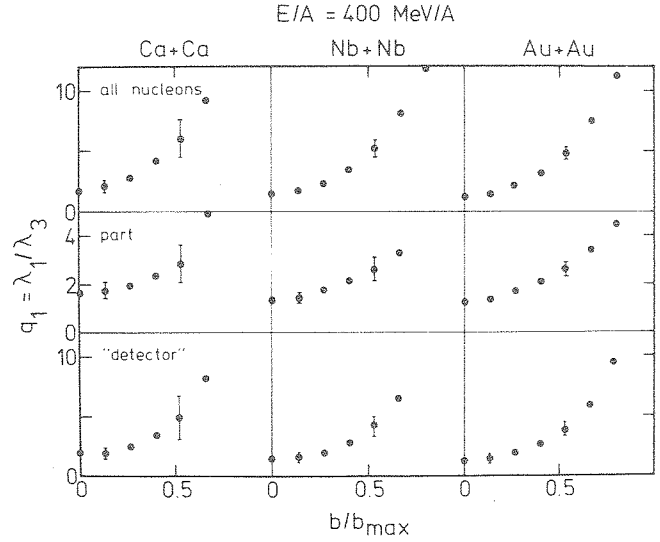

Fig. 10. INC calculation of the aspect ratio (eq. (2.3)) for several systems, as a function of the impact parameter. The upper part applies to all nucleons. The middle part corresponds to the participants, and the lower part to the events after application of the standard filter (see text). The dots give the average value and the error bars indicate the standard deviation, due to the event-by-event fluctuations.

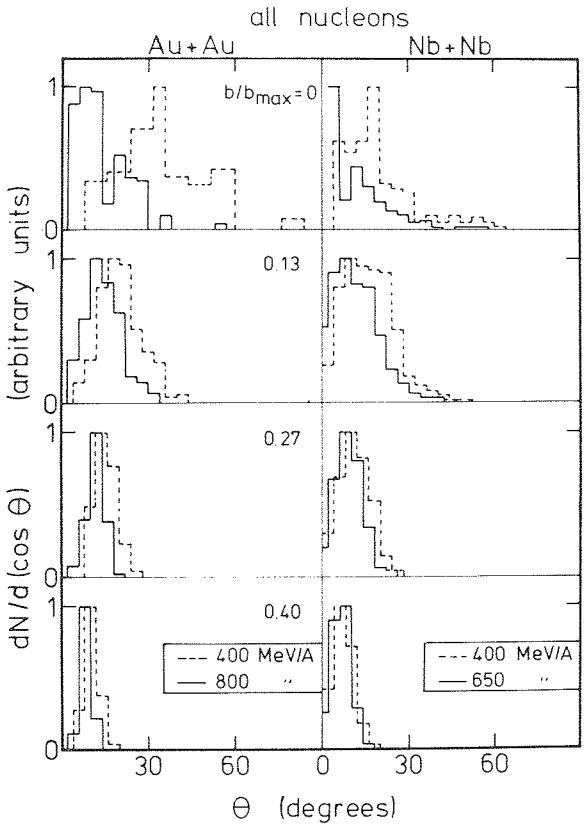

Fig. 11. INC calculation of the $dN/d\cos\theta$ distributions (for all the nucleons) for two different energies in two different systems. The distributions are normalized on the same maximum. The uncertainty of the calculation is typically the same as in fig. 6.

5. From intrinsic flow to observed flow

5.1. COMPARISON WITH EXPERIMENT

The results presented in the previous sections are not directly comparable with experiment, because the detector, here the plastic ball–wall of Berkeley, has some acceptance. Grossly speaking, it cannot detect the target spectators, nor the free neutrons and it misidentifies some particles especially at forward angles. Therefore, one has to apply some transformation to our calculated events to take the acceptance into account before comparing to experiment. Unfortunately, the acceptance of the detector, which is rather well known, cannot be applied directly to the cascade events. The main reason for this is the fact that INC is not able to predict at least directly the clusterization. To illustrate this point, the plastic ball cannot detect a free neutron, but it can detect a deuteron above a certain threshold and therefore can detect the bound neutron provided the translational energy of the latter is larger

than half the above threshold. To remedy to this situation, we have adopted the following procedure. We determine at random the free neutrons, considering that their number can be inferred from the observed deuteron/proton ratio and using the simplifying hypothesis that all clusters are deuterons. In this section, we apply to our calculated events a "standard filter" to simulate the acceptance. This standard filter is defined in ref. [16]), but for the sake of clarity we recall here its features: (i) all the nucleons of the target which have suffered a momentum transfer Δp smaller than 194 MeV/c (which corresponds roughly to an energy transfer of $\sim$20 MeV) are rejected; (ii) all the remaining nucleons with an energy $E_{\rm lab} < 20$ MeV are rejected; (iii) all the nucleons appearing at $\theta_{\rm lab} > 160°$ are excluded; (iv) a fraction of the remaining nucleons are rejected at random to simulate the free neutrons. This fraction is estimated by assuming the N/Z ratio of the retained nucleons to the same as for the original nuclei and by estimating the degree of clusterization from the observed $\tilde{d}/\tilde{p}$ ratio, as indicated above. (We give the numerical values below.)

We understand that the experimental filter has some fine details not contained in the standard filter, for instance the misidentification of particles and the so-called double hits in a single ΔE-E detector. But we adopt the point of view that the main physical effects are not contained in these details. Of course, doing so, we restrict ourselves to semi-quantitative predictions only.

Another difficulty arises from the fact that the experimental data are generally presented as $\mathrm{d}N/\mathrm{d}\cos\theta$ distributions for bins of observed charged-particle multiplicity m_c. Once again, because of the degree of clusterization, the identification between the INC output and the quantity m_c is very difficult. We therefore define a multiplicity M_ν from the INC output in the following way. We retain the number of nucleons having suffered a momentum transfer larger than p_F, the Fermi momentum, diminished by a percentage of N/A of neutrons (bound or free, this time), using the same procedure as above. This multiplicity is obviously different from m_c but, in view of the smooth behaviour of variables of this kind (see the participants in fig. 4), one expects M_ν and m_c to be smooth monotonic functions of the impact parameter and to be roughly related to each other by an overall scale factor.

Fig. 12 shows our predictions with such a procedure, and with an arbitrary choice of the lower edge of the largest multiplicity bin in Nb+Nb*. The other bins in multiplicity have been chosen to be proportional to the binning done by the experimentalists in ref. [1]). The binning for the other two systems are obtained from the Nb+Nb binning by a scaling according to the charge of the systems. Finally, the percentage of nucleons removed to account for the free neutrons is 33% for all systems. Before discussing this choice, we comment on fig. 12. Our results for Ca+Ca and Nb+Nb are in qualitative agreement with experiment [1]). The Ca+Ca system does not show a peak at finite angle for any multiplicity bin, whereas the Nb+Nb

* We choose here 68 instead of 62 in our previous work. In this way, the same cross section is contained in the largest multiplicity bin.

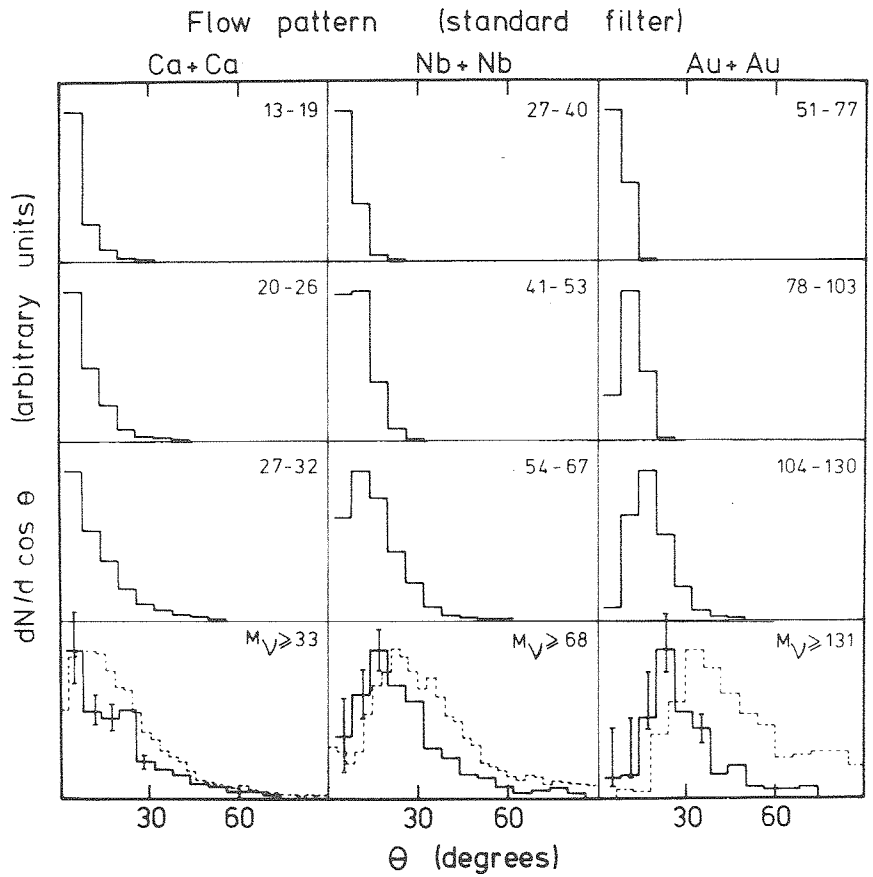

Fig. 12. INC calculation of the $dN/d\cos\theta$ distributions after application of the standard filter. The events are classified according to the multiplicity M_v, which basically is the charge carried by the participants. See text for details. The error bars indicate the uncertainty of the calculation, estimated as the square root of the counting rates. The dotted lines represent the experimental distribution for the largest multiplicity bin. For Ca + Ca and Nb + Nb, this refers to charged-particle multiplicity [1]), and for Au + Au, to the charge multiplicity, i.e. the total charge seen by the plastic ball [34]).

system displays a peak which goes to larger and larger angles for larger and larger multiplicities. At the quantitative level, our prediction for the peak angle at the largest multiplicity bin is about ~17°, smaller than the experimental value (~23°). The unfrozen version gave a peak around 24° in approximately the same conditions. The difference is due to the spurious flow of the spectators in the unfrozen version, in agreement with ref. [18]) which extensively concentrates on this point.

The difference between Ca + Ca and Nb + Nb does not come from a qualitatively different behaviour in the intrinsic flow (see fig. 7), but from the intermingling of the quantitative aspects of the intrinsic flow and the fluctuations with the distortion of the standard filter, as explained in refs. [16,28]). Essentially, the filtering introduces

a stronger dispersion of the dots in fig. 7 and a displacement of their barycenter towards the right of the figure. This is mainly a result of the removal of the target spectators. When present, the latter tends to align the sphericity tensor with the beam. For Nb+Nb, the points are sufficiently on the right and the dispersion is sufficiently small to guarantee a definite peak in the $dN/d\cos\theta$ distribution (see sect. 4 and appendix B for the connection between fig. 7 and the $dN/d\cos\theta$) for the largest-multiplicity bins. The latter roughly correspond to small impact parameters. For Ca+Ca, the fluctuations that are linked to the number of participants, as we recall, are strong enough to wash out the intrinsic flow. For the Au+Au system, the situation is more pronounced than for Nb+Nb, as expected from fig. 7 and fig. 8.

5.2. SENSITIVITY OF THE NUMERICAL RESULTS

We now discuss the sensitivity of our results on the arbitrarinesses that we introduced in constructing fig. 12. We first examine the sensitivity to the number of removed neutrons. This is shown for the Nb+Nb system at the top of fig. 13. The largest percentage (36.9%) was used in our previous work [16]), but the recently published values of the $\tilde{d}/\tilde{p}$ ratio [29]) seem to favour a somewhat lower value (33%). If the percentage is still lowered, the peak seems to survive, but its definition is somewhat less clear due to the large statistical fluctuations arising in the population of the first channels (small-θ angles).

Another interesting feature is contained in the middle and the lower parts of fig. 13, which shows $\tilde{\theta}$, the average over $dN/d\cos\theta$ considered as a function of θ, i.e.

$$\tilde{\theta} = \frac{\int_0^{\pi/2} \theta (dN/d\cos\theta)\, d\theta}{\int_0^{\pi/2} (dN/d\cos\theta)\, d\theta}, \tag{5.1}$$

and the true average angle,

$$\langle\theta\rangle = \frac{\int_0^{\pi/2} \theta (dN/d\cos\theta) \sin\theta\, d\theta}{\int_0^{\pi/2} (dN/d\cos\theta) \sin\theta\, d\theta}, \tag{5.2}$$

respectively. These quantities are calculated for the largest multiplicity bin, as a function of $M_{\nu L}$, the lower boundary of the bin. For all the percentages P_n of the removed neutrons investigated, both $\tilde{\theta}$ and $\langle\theta\rangle$ increase with $M_{\nu L}$, showing that the flow and the multiplicity are correlated. There is a sizeable sensitivity to P_n for the largest multiplicities only (≥ 70). The sensitivity of $\tilde{\theta}$ does not seem to follow a regular pattern, whereas that of $\langle\theta\rangle$ does. This is particularly visible for $P_n = 29.5$. Actually, this happens because $\tilde{\theta}$ weights much more the small angles where the

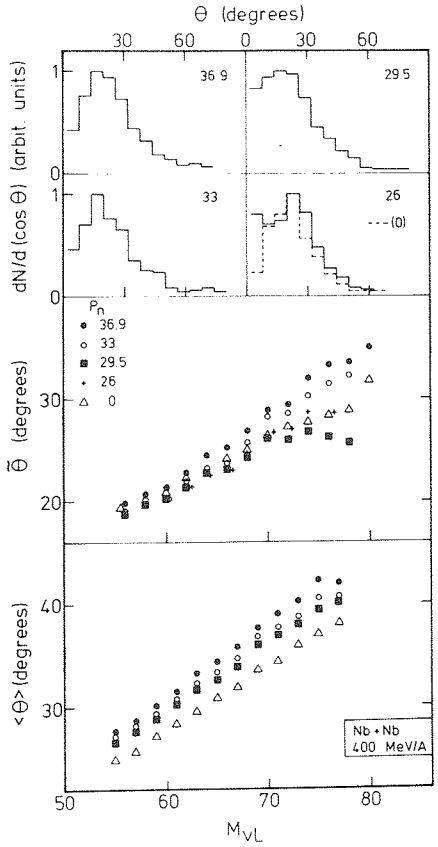

Fig. 13. Nb + Nb system at 400 MeV/A: sensitivity of the calculated results upon the main parameters of the filter. The upper part of the filter gives the $dN/d\cos\theta$ distribution for the largest multiplicity bin for several values of the percentage P_n of removed neutrons. The lower part gives the average value of θ as a function of P_n and of the threshold value M_{VL} determining the largest multiplicity bin. The middle part gives a mean θ-value using the weighting function $1/\sin\theta$. See text for details.

population is accidentally small for that value of P_n. Let us notice that both $\langle\theta\rangle$ and $\tilde{\theta}$ are larger than the peak position. All these quantities vary qualitatively in the same way as P_n and M_{VL} are varied. However, the peak position is more subject to local fluctuations of the θ-distribution.

We have also investigated the sensitivity upon the cut in momentum transfer. We made a calculation with a cut equal to 168 MeV/c and to 217 MeV/c instead of 194 MeV/c, which roughly correspond to a transfer in energy of 15 and 24 MeV, respectively. We did not observe significant differences as far as the peak position is concerned. The value of $\langle\theta\rangle$ changes by 2° between these two values.

Finally, we would like to mention that a filter on the momentum transfer, such as the one used here, removes more nucleons in the target fragmentation region than a filter on the final kinetic energy for the same threshold energy. This has a

non-negligible effect on the flow. For instance, concerning the largest multiplicity bin in Nb + Nb, the average $\langle\theta\rangle$ changes from 25.7° to 20°. We emphasize, however, that the filter on the momentum transfer is more reasonable, since it is hardly acceptable that a nucleon experiences individually a small momentum transfer. In this case, very likely, it will stick rather with the remaining target nucleons.

5.3. DISCUSSION

The lower part of fig. 13, as well as fig. 12, call for some remarks concerning the comparison with experiment. With the value of $M_{\nu L}$ adopted in fig. 12 and the standard filter, we obtain a flow angle which is already too small compared to experiment (17° instead of 23° for Nb + Nb). But we have introduced some arbitrariness in choosing $M_{\nu L} = 68$. If the latter was chosen smaller but within reasonable values, say between 54 and 68, the qualitative result of fig. 12 is preserved. But quantitatively, it is clear that the peak position of the largest multiplicity bin would be shifted to smaller angles. Furthermore, it seems that the double hits, neglected in our analysis, are not at all infrequent [30]). Since they are thrown away in the experimental analysis, they would influence our estimate of the flow angle. They will do it in two somewhat mutually compensating ways. If we throw away participants, this will reduce the flow. However, double hits are more frequent in the forward direction, and throwing these away will increase the flow. It is quite clear to our mind that our cascade model lacks some flow, but due to the delicate application of the filtering, it is hard to quantify this lack of flow. Despite this, we present at the bottom of fig. 12 a comparison with experiment. This should be considered as probably the most favorable comparison for our cascade model. The lack of flow, between 5° to 10° for both Nb + Nb and Au + Au, is the *minimum* room

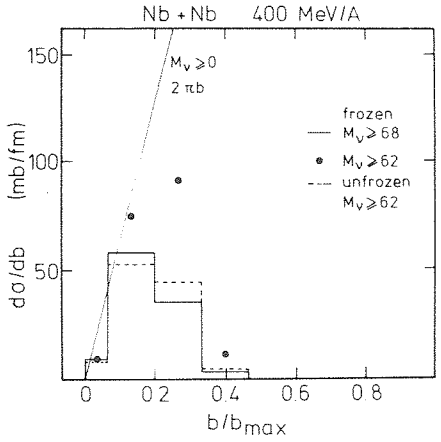

Fig. 14. Impact parameter distribution (full lines) of the events contained in the largest multiplicity bin in Nb + Nb at 400 MeV/A (central part of fig. 12). Comparison is made with other binnings and with the case of no multiplicity selection (straight line).

left for the physics associated with mean fields and the equation of state. This might appear small but it will probably turn out to be significant.

The indeterminacy of the proper choice of $M_{\nu L}$ would be removed, or at least reduced, if the cross sections corresponding to the multiplicity bins were known experimentally. We give our prediction for this quantity in fig. 14, as well as the splitting according to the contributing impact parameters. It can be seen that the most important impact parameters are around 0.2 of b_{max} and not zero. We mention that Kitazoe *et al.*[24]) find a similar effect, even more accentuated, since they find a maximum around $b/b_{max} = 0.3$. The integrated cross section is about 5% of the geometrical cross section.

6. What is causing the flow?

6.1. THEORETICAL CONSIDERATIONS

The INC model has the defect of its simplicity, and of simulations in general: the link between physical effects and their causes is far from transparent. It is therefore useful to look at the Landau-Vlassov equation which embodies essentially the same physics, but which has the virtue of being an equation. It can be written (in the non-relativistic form) as

$$\left(\frac{\partial}{\partial t}+\frac{\boldsymbol{p}}{m}\cdot\nabla-(\nabla U)\cdot\nabla_p\right)f_1(\boldsymbol{r},\boldsymbol{p},t)$$
$$=\int\frac{\mathrm{d}^3p_1}{(2\pi)^3}\frac{\mathrm{d}^3p_2}{(2\pi)^3}\frac{\mathrm{d}^3p_3}{(2\pi)^3}\,W(\boldsymbol{p},\boldsymbol{p}_1\to\boldsymbol{p}_2,\boldsymbol{p}_3)(\tilde{f}_2\tilde{f}_3-\tilde{f}\tilde{f}_1)\,. \tag{6.1}$$

In this equation, which governs the evolution of the one-body distribution function $f_1(\boldsymbol{r},\boldsymbol{p},t)$, the r.h.s. member describes the effect of the collisions and the particles are assumed to be moving in a field U, which can be an external or a self-consistent field. Here, we restrict ourselves to Hartree-type fields

$$U=U(\rho(\boldsymbol{r}))\,. \tag{6.2}$$

The quantity W is the probability for two particles with momenta $\boldsymbol{p}$ and $\boldsymbol{p}_1$ to collide and to have momenta $\boldsymbol{p}_2$ and $\boldsymbol{p}_3$ in the final state. The quantities $\tilde{f}_i$ are defined by

$$\tilde{f}_i=(2\pi)^{-3}f_1(\boldsymbol{r}_i,\boldsymbol{p}_i,t)\,. \tag{6.3}$$

In eq. (6.1), the quantum statistics is neglected, but all the below can be extended to an Uehling-Uhlenbeck collision term which accounts for the statistics.

The INC model does not contain a mean field (in its simplest version) but, in some sense, it is a more general theory than the Landau-Vlassov equation, because it can describe the evolution of the 2-body, 3-body... distribution functions, and does not rely on the molecular-chaos hypothesis. Furthermore, our calculation includes pions and Δ's, which may be of importance for the flow. Here, however, we disregard these aspects for simplicity.

The Landau-Vlassov equation is a complicated equation. An insight into the underlying physics can be gained by looking at the moments (in $\boldsymbol{p}$) of the equation, anticipating that the first moments are the most important ones. Furthermore, it is the usual framework in which to discuss the connection with hydrodynamics. We closely follow here the presentation of ref. [31]).

The zeroth-moment equation is simply the continuity equation

$$\frac{\partial \rho}{\partial t} + \nabla \cdot (\rho \boldsymbol{u}) = 0 , \tag{6.4}$$

where

$$\rho = \int \mathrm{d}^3 p \, f_1(\boldsymbol{r}, \boldsymbol{p}, t) . \tag{6.5}$$

The quantity

$$\boldsymbol{u} = \frac{1}{\rho} \int \mathrm{d}^3 p \, \boldsymbol{p} f_1(\boldsymbol{r}, \boldsymbol{p}, t) \tag{6.6}$$

can be interpreted as the collective or macroscopic velocity. The second moment of the one-body distribution,

$$\tau_{ij} = \int \mathrm{d}^3 p \, p_i p_j f_1(\boldsymbol{r}, \boldsymbol{p}, t) , \tag{6.7}$$

can be related to the average (over the runs) sphericity tensor (eq. (2.1)) by the relation

$$Q_{ij} = \frac{1}{2m} \int \mathrm{d}^3 r \, \tau_{ij} , \tag{6.8}$$

the equality being understood as taken at late times, when the collision process has ceased. Writing

$$\boldsymbol{p} = m\boldsymbol{u} + \delta \boldsymbol{p} , \tag{6.9}$$

the tensor τ_{ij} can be split into two parts:

$$\tau_{ij} = R_{ij} + S_{ij} , \tag{6.10}$$

with

$$m^{-2} R_{ij} = \rho u_i u_j \tag{6.11}$$

and the stress tensor

$$S_{ij} = \int \mathrm{d}^3 p \, \delta p_i \, \delta p_j f_1(\boldsymbol{r}, \boldsymbol{p}, t) . \tag{6.12}$$

The tensor R_{ij} embodies the collective flow whereas the stress tensor S_{ij} can be understood as the internal flow tensor density. With these notations, the first-moment equation is

$$\rho\left[\frac{\partial u}{\partial t}+\boldsymbol{u}\cdot\boldsymbol{\nabla}\boldsymbol{u}\right]+\boldsymbol{\nabla}\cdot\boldsymbol{\Pi}=0\,, \tag{6.13}$$

where the tensor Π_{ij} is

$$\Pi_{ij}=S_{ij}+\delta_{ij}(\rho U-V) \tag{6.14}$$

with

$$V[\rho]=\int_0^{\rho} U(\rho')\,\mathrm{d}\rho'\,. \tag{6.15}$$

The second-moment equation can be split into two equations:

$$\frac{\partial R_{ij}}{\partial t}+\boldsymbol{\nabla}\cdot(\boldsymbol{u}R_{ij})+u_i\sum_k\nabla_k\Pi_{kj}+u_j\sum_k\nabla_k\Pi_{ki}=0\,, \tag{6.16}$$

$$\frac{\partial S_{ij}}{\partial t}+\boldsymbol{\nabla}\cdot(\boldsymbol{u}S_{ij})=-\sum_k(S_{ik}\nabla_k u_j+S_{jk}\nabla_k u_i)-S_{ij}\boldsymbol{\nabla}\cdot\boldsymbol{u}$$
$$-\sum_k\nabla_k\mathcal{J}_{k,ij}+\int\mathrm{d}^3p\,\delta p_i\,\delta p_j\,\mathrm{I}\,. \tag{6.17}$$

In the last equation, I stands symbolically for the collision term (r.h.s. of eq. (6.1)) and the tensor $\mathcal{J}_{k,ij}$ is given by

$$\mathcal{J}_{k,ij}=\int\mathrm{d}^3p\,\delta p_i\,\delta p_j\,\delta p_k f_1(\boldsymbol{r},\boldsymbol{p},t)\,. \tag{6.18}$$

Usually, only eq. (6.17) is written down. In fact, eq. (6.16) is a direct consequence of the first-moment equation (6.13).

Before entering into detailed considerations, we would like to make two remarks.

(i) The physics contained in eqs. (6.16) and (6.17) is particularly transparent: the evolution of the internal stress tensor is governed by itself and by the collisions. In turn, the stress tensor acts as a driving term for the evolution of the collective flow tensor R_{ij}.

(ii) The mean field (more precisely, the density dependence of the mean field) is another source for the time evolution of the collective flow tensor. But both causes are *qualitatively of equal importance*: they are treated on the same footing in eq. (6.16).

6.2. SOME LIMITS

The simplest limit is the ideal fluid hydrodynamics which corresponds to local equilibrium (the last term in (6.17) always vanishes) and to a stress tensor which

reduces to a single number on the diagonal:

$$S_{ij} = p_{\mathrm{th}}\,\delta_{ij}\,. \tag{6.19}$$

In this case, eqs. (6.16) and (6.17) become

$$\frac{\partial R_{ij}}{\partial t} + \nabla\cdot(\boldsymbol{u}R_{ij}) + u_i\nabla_j p + u_j\nabla_i p = 0\,, \tag{6.20}$$

$$\frac{\partial p_{\mathrm{th}}}{\partial t} + \nabla\cdot(\boldsymbol{u}p_{\mathrm{th}}) = -p\tfrac{5}{3}\nabla\cdot\boldsymbol{u}\,, \tag{6.21}$$

where

$$p = p_{\mathrm{th}} + (\rho U - V) = p_{\mathrm{th}} + p_{\mathrm{int}}\,. \tag{6.22}$$

The quantity p_{th} is the thermal pressure and p can be considered on the total pressure. Indeed, if U depends upon the density only, one can write

$$p_{\mathrm{int}} = \rho^2\frac{\partial^2(\mathscr{H}_{\mathrm{int}}/\rho)}{\partial\rho^2}\,, \tag{6.23}$$

where $\mathscr{H}_{\mathrm{int}}$ is the interaction energy density. Comparison of eqs. (6.22) and (6.23) leads to

$$\mathscr{H}_{\mathrm{int}}(\rho) = V(\rho)\,. \tag{6.24}$$

If $U(\rho) = U_0\rho$, this energy density reduces to the well-known Hartree form

$$\mathscr{H}_{\mathrm{int}}(\rho) = \tfrac{1}{2}U_0\rho^2\,. \tag{6.25}$$

Note that, once again, the thermal pressure and the interaction pressure have the same status: both act as a driving force for creating the collective flow. The building up of the thermal pressure comes from the divergence of the velocity field. If the hydrodynamical limit is taken literally, the sphericity tensor would be given by the tensor R_{ij} alone, because at the end of the collision process the matter is decompressed and $p_{\mathrm{th}}\to 0$. In this pure "bulk" limit, there is a kind of scaling invariance. If the fields $\Phi(\boldsymbol{r}, t)$, where Φ stands for ρ, p, $\boldsymbol{u}$ and R_{ij}, are solutions of eqs. (6.4), (6.13), (6.20), the fields

$$\Phi_{\mathrm{sc}} = \Phi(\Lambda\boldsymbol{r}, \Lambda t) \tag{6.26}$$

are also a solution provided, of course, that the initial conditions ($t = 0$) can be obtained by the same scaling transformation. The latter is indeed realized when going, for instance, from the Ca + Ca to the Au + Au case at the same initial velocity, i.e. the same energy per nucleon, and at the same $b/b_{\max}$ ratio. The parameter Λ is then simply the ratio between the Au and Ca radii. This scaling law, observed in

another way in ref. [32]), is known in similarity theory [33]) to arise from the Strouhal number $[S]$:

$$[S]=\left[\frac{u\tau}{l}\right], \tag{6.27}$$

where u, l and τ are the characteristic velocity, length and time of the system, respectively. Of course, as indicated by eqs. (6.26) and (6.27), the similarity holds for a corresponding scale in time: the tensor R_{ij} for Au+Au can be obtained by the scaling of R_{ij} for Ca+Ca, but this correspondence implies a later time for the former system as compared to the latter. In usual hydrodynamical calculations this scaling law is not expected to hold completely. The reason is that the evolution is stopped at some freeze-out time, which may not respect the scaling law. Note, however, that if the freeze-out is determined by reaching a given density, the scaling law should still hold. Experimentally [2,34]), this scaling law does not seem to be valid, but the efficiency of the apparatus may introduce some uncertainty as well.

The next possible limit, namely viscous hydrodynamics, exhibits another source for the collective flow. The stress tensor takes the form

$$S_{ij}=p_{\mathrm{th}}\,\delta_{ij}-\eta(\nabla_j u_i+\nabla_i u_j-\tfrac{2}{3}\delta_{ij}\nabla\cdot\boldsymbol{u})\,. \tag{6.28}$$

We retain here only the shear viscosity. Eq. (6.16) becomes

$$\frac{\partial R_{ij}}{\partial t}+\nabla\cdot(\boldsymbol{u}R_{ij})+(u_i\nabla_j+u_j\nabla_i)p-\eta[u_i\Delta u_j+u_j\Delta u_i$$

$$+\tfrac{1}{3}(u_i\nabla_j+u_j\nabla_i)\nabla\cdot\boldsymbol{u}]=0\,. \tag{6.29}$$

Eq. (6.17) becomes very complicated already in this limit and is not interesting for our purpose. Here the viscosity is expected to damp the momentum flow: it opposes itself to the work done by the pressure. With the addition of the viscosity terms, the scaling law discussed above breaks down. The fact that the results of our INC calculations (and probably experiment as well) do not follow the scaling law indicates that we are perhaps witnessing viscosity effects. A similar analysis has already been performed by Jaqaman and Mekjian [35]).

Viscous (and non-viscous) hydrodynamical equations are strictly valid for a system of point-like particles if they are intended to describe evolution of disturbances whose characteristic lengths (and times) are larger than the thermalisation mean free path (and lifetime). In a very extended system it is generally possible to define a scale which is small compared to the dimension of the system and large compared to the mean free path. In other words, it is generally possible to divide the space into cells with dimension larger than the mean free path and much smaller than the system size. The various physical quantities vary gently from cell to cell and can be handled by the hydrodynamic equations. In the heavy-ion case, the situation is much less favourable. The thermalisation mean free path is not small compared to

the radius of the nuclei we investigate in this paper. Therefore it is expected that the stress tensor will not be of the form (6.19) or (6.28).

In all generality, one can write

$$S_{ij} = \tfrac{1}{3}(\mathrm{tr}\, S)\delta_{ij} + \tilde{S}_{ij}\,, \tag{6.30}$$

where $\tilde{S}$ is called the deviator. We still call $p = \frac{1}{3}\,\mathrm{tr}\,\Pi$. One may then write

$$\frac{\partial R_{ij}}{\partial t} + \nabla\cdot(\boldsymbol{u}R_{ij}) + (u_i\nabla_j + u_j\nabla_i)p + \sum_k (u_i\nabla_k\tilde{S}_{kj} + u_j\nabla_k\tilde{S}_{ki}) = 0\,, \tag{6.31a}$$

$$\frac{\partial p}{\partial t} + \nabla\cdot(\boldsymbol{u}p) = -\tfrac{5}{3}p\nabla\cdot\boldsymbol{u} - \tfrac{2}{3}\sum_i\sum_k \tilde{S}_{ik}\nabla_k u_i + \tfrac{1}{3}\int \mathrm{d}^3p(\delta p)^2\mathrm{I}\,, \tag{6.31b}$$

$$\frac{\partial \tilde{S}_{ij}}{\partial t} + \nabla\cdot(\boldsymbol{u}\tilde{S}_{ij}) = -\tfrac{5}{3}\tilde{S}_{ij}\nabla\cdot\boldsymbol{u} + \int \mathrm{d}^3p[\delta p_i\,\delta p_j - \tfrac{1}{3}(\delta p)^2]\mathrm{I}\,, \tag{6.31c}$$

where we have neglected the $(\delta p)^3$ term, because it is really too complicated to handle. If one is not too far from local equilibrium, the last term in (6.31a) is expected to behave like the usual viscosity term. We focus now on the deviator. If departure of local equilibrium is sufficient, the leading term in (6.31c) will be the collision term and the deviator will never go to zero. This should happen in the heavy-ion case, since some nucleons make one or two collisions. We make a relaxation time approximation to clarify the physical meaning of eq. (6.31c):

$$\left(\frac{\partial}{\partial t} + \boldsymbol{u}\cdot\nabla\right)\tilde{S}_{ij} \approx -\tilde{S}_{ij}/\tau_{\mathrm{rel}}\,. \tag{6.32}$$

The solution of this equation can be written as

$$\tilde{S}_{ij} = \tilde{S}_{ij}(t=0)\exp(-t/\tau_{\mathrm{rel}})\,, \tag{6.33}$$

where the evolution should be understood to occur along a velocity field line. $\tilde{S}_{ij}(t=0)$ can be considered as the deviator when the nuclei start to interpenetrate each other. It is thus a strongly elongated tensor along the beam direction. The deviator influences the flow, because it enters into eq. (6.31a), but also because, in the microscopic view, it is not necessarily vanishing at the end of the collision process and therefore should be added to R_{ij} to calculate the average sphericity tensor. Eq. (6.33) explicitly shows that the final flow can be influenced by the parameter $y = \tau/\tau_{\mathrm{rel}}$. The latter is roughly proportional to the inverse of

$$y = \lambda/R\,. \tag{6.34}$$

Here, τ is the same as in eq. (6.27), λ is the thermalization mean free path, and R is the radius of the system. These qualitative considerations show that, if the collective flow is influenced by off-equilibrium effects, it should be governed to some extent by the parameter y. If y increases, $\tilde{S}$ is more important and the flow is reduced. Note finally that, grossly speaking, y increases with energy (in the 400 MeV/A – 1 GeV/A range) and decreases with the size of the system.

6.2. FLOW INSIDE THE INC MODEL

Can the flow inside the intranuclear cascade be understood in terms of the preceding discussion? To try to answer this question, we make the following observation. In fig. 15, we have plotted in the upper part the density at the c.m. of the Au+Au system and in the lower part the flow angle, i.e. the angle between the largest axis of the sphericity tensor and the beam axis. It is clear that the final flow angle is reached at the end of the compression stage. In this perspective, it is quite instructive to look at fig. 16. The flow grows in the time span during which the "spectator caps" (i.e. those parts of the target (projectile) which in their original motion do not intercept the target (projectile)) are passing close by the central participants region. Therefore, it is quite natural to consider that the flow originates from the work done by the pressure built by the compression into the participant system on the "caps", in a very similar way as in hydrodynamics. There is an important difference, however. Inside the cascade, the pressure force does not act coherently on the spectators, but rather through two-body collisions. An obvious consequence of this is that there are true spectators inside the cascade. Some nucleons have escaped from interacting with nucleons of the central zone and propagate undisturbed in the beam direction. This is particularly visible in fig. 16.

If the pressure was the sole cause of the flow (i.e. if eq. (6.20) was the only relevant equation), the flow would be the same for each of the Ca+Ca, Nb+Nb and Au+Au systems as we have already noticed. Neither the reality nor our calculation indicate such a thing. The next possible (simple) cause would be the

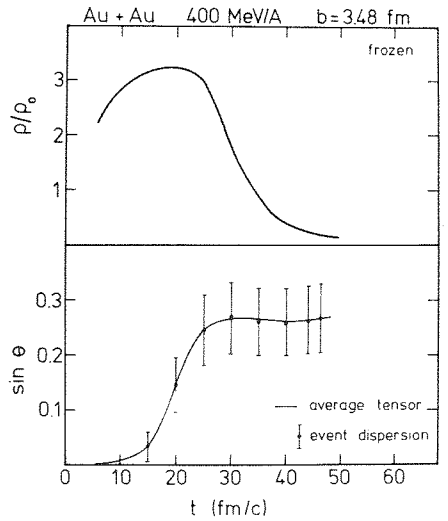

Fig. 15. Time evolution of the c.m. density (in units of ρ_0, the normal nuclear matter density) and of the angle in the c.m. system between the largest axis of the sphericity tensor (eq. (2.2)) and the beam axis. The continuous line corresponds to the tensor calculated by summing over all the events. The dots give the average of the angle calculated event by event. The error bars give the event-by-event fluctuations.

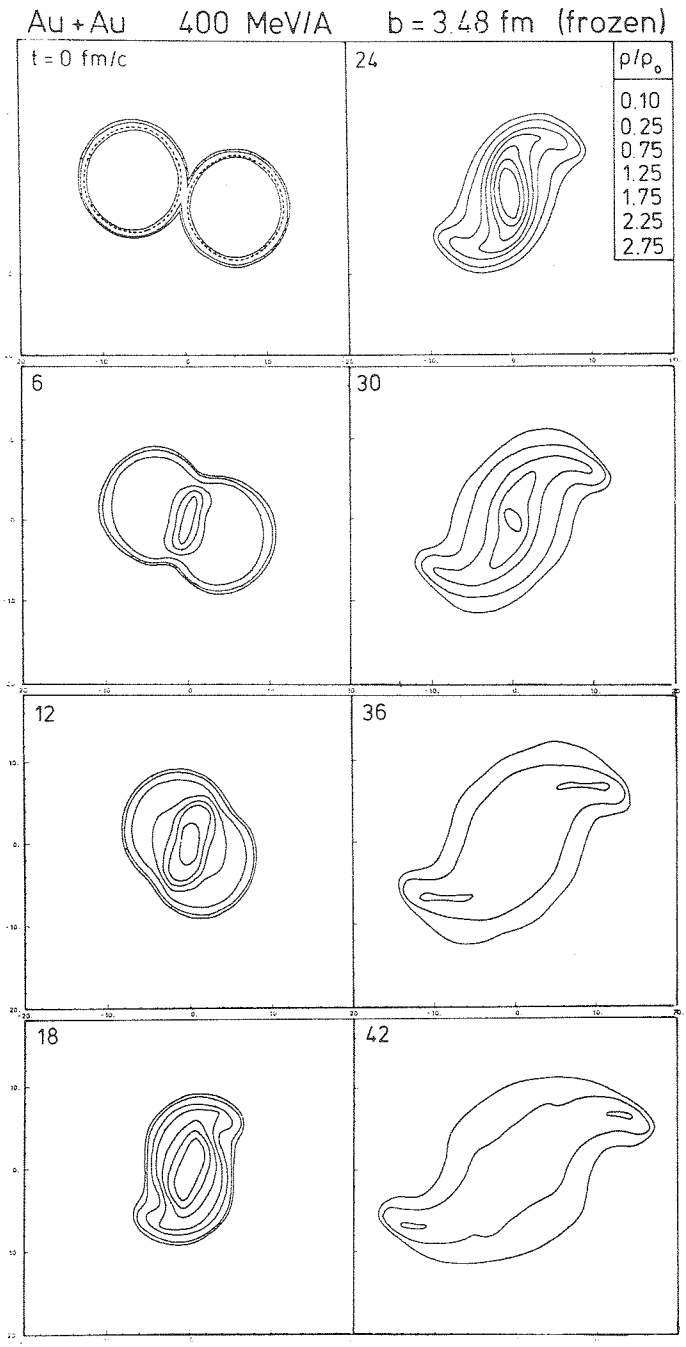

Fig. 16. Time evolution of the baryon density in the reaction plane for the Au + Au system at 400 MeV/*A*. The full curves are isodensity curves in the c.m. system and correspond to the numerical values given in the insert of the upper-right corner, starting from outside the system. The incident nuclei are originally running towards each other along the horizontal direction.

viscosity forces (eq. (6.29)). Is there any feature in the cascade that can be understood as coming from this cause? Fig. 17 would suggest a positive answer. It displays the mass current at about the maximum density in the Nb + Nb system. Clearly, matter is deviated in the perpendicular direction. But, and this seems to emerge also from a careful analysis of fig. 15, the different layers do not have the same perpendicular velocity. Therefore, it is expected that the viscosity plays a role. Most likely, the viscosity forces tend to oppose to the rise of the flow, since they will slow down the elements of matter which have the largest velocity at the time indicated in fig. 16.

It is not easy to determine clearly how the viscosity forces influence the mass and energy dependence of the flow. It is argued in ref. [36]) that the viscosity forces reduce the flow [see also ref. [35])] and that the resulting flow decreases with decreasing size of the system and with increasing incident energy. The latter statement can be roughly understood as being due to the general increase of the viscosity coefficient η (eq. (6.29)) with the temperature. The variation with the mass of the system can be understood by a dimensional analysis of the viscosity term in eq. (6.29). The velocity field being roughly scaled (exactly in the limit $\eta \to 0$ as we have seen), this term behaves like R^{-2}, where R is the radius of the nucleus (Ca, Nb or Au). Now, this term expresses the density of power dissipated by the friction forces. In other

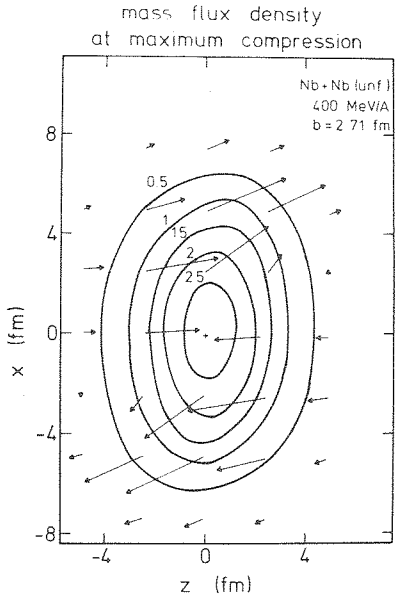

Fig. 17. Distribution of the mass flux density (ρu in eq. (6.4)) as viewed in the c.m. system at about the time of maximum compression. This figure refers to the reaction plane of the Nb + Nb system at the impact parameter $b = 2.71$ fm. The arrows give the direction and the intensity (proportional to their length) of the mass-flux density vector at the points they are attached. The full curves are isodensity curves. The numbers give the ratio of the baryon density to the normal nuclear matter density. The nuclei are originally running towards each other along the z-direction. The small cross is the location of the c.m. of the system.

words, the contribution of the viscous forces to Q_{xz} can be written as

$$Q_{xz}^{(v)} = \int \mathrm{d}t \int \mathrm{d}^3 r[\text{term in } \eta]\,. \tag{6.36}$$

Therefore $Q_{xz}^{(v)}$ is expected to behave like

$$Q_{xz}^{(v)} \sim R\tau\,, \tag{6.37}$$

where τ is the typical collision time, or in the limit of small η (see the discussion about similarity)

$$Q_{xz}^{(v)} \sim R^2\,. \tag{6.38}$$

Actually, in our calculation, we observe an almost perfect proportionality between R and τ. Now, the mass dependence of Q_{zz} is expected to be simply as R^3, because e.g. in the thermal limit $Q_{zz} \approx \frac{1}{3} A u_0^2$, where A is the mass of the system and where u_0 is the initial c.m. velocity. The flow angle which increases with the ratio Q_{xz}/Q_{zz} will be reduced by the viscosity force by an amount proportional to R^{-1}. In other words, the flow angle should increase with the mass of the system.

In conclusion, the mass and energy dependence of the flow, qualitatively the same in the cascade and in nature, can be qualitatively understood as arising from the contradictory effects of the pressure and the viscosity forces.

In the cascade, however, there is no doubt, due to the very presence of the spectators, that off-local-equilibrium effects are important. It is impossible to discriminate between viscosity effects and general off-equilibrium effects on the basis of the mass and energy dependence. For the latter, eq. (6.33) is relevant. As the mass increases, off-equilibrium effects are reduced. As the energy increases, the thermalisation mean free path increases mainly because in the 250–800 MeV range the differential nucleon–nucleon cross section is more and more forward-peaked. In order to really separate viscosity and more general off-equilibrium effects, one has to look carefully at the structure of the stress tensor. We are currently pursuing this analysis within the INC model.

7. Discussion: conclusion

We have shown that there is definitely an intrinsic collective flow in our INC model. This raises several questions in view of other works along the same lines. It has been stated that the Yariv and Fraenkel cascade cannot generate a flow. However, the question of the intrinsic flow (disregarding the filtering procedure) has not been studied yet, as far as we know. Therefore, it is hard to compare the two cascades from this point of view. The same remark applies to the Kitazoe cascade, since in ref. [24]) only filtered results are shown.

The comparison on the filtered results is very hard to make, because of the reasons we mentioned in sect. 5, namely that the filter applied to plastic ball events is not

directly applicable to cascade events, because of clusterization. It is very hard to know exactly the detail of the filter applied in ref. [1]) to the Yariv-Fraenkel cascade events, but the filter is undoubtedly more refined than our standard filter. As for the Kitazoe cascade, we do not know how their filter compares to ours. To quote ref. [24]), they state that "the experimental condition of the Plastic Ball and the Wall was rigorously taken into account for the solid angles and the energies of ejected protons and pions with the aid of a Fortran program provided by one of the authors of Ref. [1])". They do not, however, say anything about the clusterization problem. One can thus see how difficult a comparison between the three codes is. Our impression however, is, that the flow in our cascade is larger than in the Yariv and Fraenkel one and smaller than in the Kitazoe one. This brings us to the causes of the flow. We think that there is more pressure in our cascade than in the Yariv and Fraenkel one, because in the latter the cascade-cascade interaction is such that a given cascading particle sees the other cascading particles as a continuous medium. The momentum content of this medium follows the Fermi gas law and therefore can be much lower than for the original cascading particles. As a consequence, the pressure may be smaller. The Kitazoe cascade seems to be very similar to our own cascade, as far as the central interaction region is concerned, but introduces a new feature, namely the possibility for a central region particle to push on the spectator zone as a whole. There are no true spectators in their cascade, in the sense of a particle keeping its original momentum for ever. To use the conventional jargon, the flow in their cascade comes from a side-splash and from a bounce-off, whereas ours strictly contains a side-splash only. However, if one considers nucleons experiencing a small momentum transfer as a spectator, our cascade contains a bounce-off as well. We do not pretend that we fully understand the comparison between the three codes, because this would require a detailed knowledge of the numerical codes, but we want to present our opinion as an attempt to clarify a rather confused situation.

It may appear strange to some people that the cascade, basically a single-particle model, can generate a collective behaviour. We have shown on very general grounds that the collective flow results from the work done by the pressure forces. Since there is some pressure built inside the cascade, there is no *a priori* reason for not having a collective flow. Yet, it might appear disturbing to have a collectivity generated by a pressure which, in a sense, embodies the local disorder. However, the collectivity here does not arise from nothing, but is already present in the ordered motion in the initial state. As eq. (6.20) suggests, the collective flow comes from the pressure work on the ordered motion of the spectator "caps", following our terminology of sect. 6.

Perhaps the analysis through study of the orientation of the sphericity tensor of the filtered events is not the most appropriate one to exhibit the presence or the absence of the collective flow. In this perspective, it seems that the transverse momentum analysis of Danielewicz and Odyniec [37]) is much more suited. We did

not try such an analysis here, but we give in fig. 18 the mean transverse momentum in the reaction plane as a function of the longitudinal momentum (for unfiltered events and using the theoretical reaction plane). Clearly, this method reveals a definite flow in the cascade. Fig. 18 also shows that the transverse momentum content is practically fixed at the end of the compression stage (see fig. 16).

When we apply our "standard" filter, we get a flow which is smaller than the experimental one (see fig. 12). To quantify the lack of flow is a very hard task. It involves the handling of delicate questions, such as the problem of the double hits and of the misidentification at very forward angles [see ref. [18])]. But it is certain that our INC model predicts too small flow angles.

What is missing from the cascade? As we explain in sect. 6, the flow results from the action of the pressure forces and is reduced by viscosity forces and/or by more important off-equilibrium effects. Therefore, either the cascade pressure is not large enough or the viscosity forces or the off-equilibrium effects are too strong. If one compares with hydrodynamics [38]), which contains only pressure and viscosity forces, it seems that the difference from our present calculation can be understood as arising from smaller viscosity forces in hydrodynamics [39]). We have seen that the off-equilibrium effects, viscosity or more important effects, qualitatively explain the mass and energy dependence of the flow. This would incline us to believe that the pressure forces inside the cascade are not strong enough, which is an indication of a stiffer equation of state [40]). Recent works based on the numerical solution of

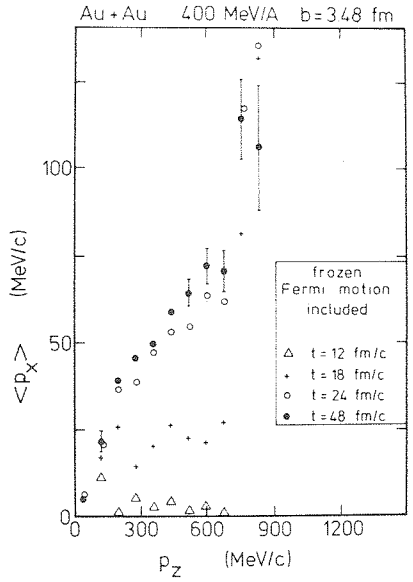

Fig. 18. Au + Au system at 400 MeV/A. Time evolution of the mean transverse momentum projected on the reaction plane as a function of the c.m. longitudinal momentum. See text for details. Only the forward hemisphere in the c.m. frame ($p_z > 0$) is shown. The error bars give the typical uncertainty of the calculation.

Landau-Vlassov equations [40-43]) are in favour of such an explanation. However, only a detailed analysis of the mass and energy dependence can help us to understand whether the off-equilibrium effects are correctly described by the usual collision regime.

We are very grateful to Prof. J.P. Alard and Dr. G. Montarou from the LPC of Clermont-Ferrand for their valuable help in the computation work. We would like to thank Drs. H. Stöcker, H.-Å. Gustaffson and H.-G. Ritter for helpful discussions. We are particularly grateful to Drs. M. Gyulassy and K. Frankel for helping us to clarify the problem of the freezing. One of us (J.C.) is very grateful to the members of the DPhN-ME of Saclay for their kind hospitality.

Appendix A

ESTIMATE OF THE STATISTICAL ERRORS

Let y_n denote the value of a calculated variable (e.g. the aspect ratio) at the nth run. This quantity can be considered as a stochastic variable of the mean $\bar{y}$ and of the variance σ^2. Then, according to the central-limit theorem,

$$y_e = \frac{1}{N} \sum_{n=1}^{N} y_n \tag{A.1}$$

can be regarded as a stochastic variable with mean $\bar{y}$ and with variance σ^2/N, where N is the number of runs, provided there is no correlation between the y_n's. Similarly, the quantity

$$\sigma_e^2 = \frac{1}{N-1} \sum_n (y_n - y_e)^2 = \frac{N}{N-1} \left[\frac{1}{N} \sum_n y_n^2 - \bar{y}_e^2 \right] \tag{A.2}$$

is a stochastic variable with mean σ^2 and with variance $2\sigma^4/N$, if the distribution of y_n is sufficiently close to a gaussian distribution. Symbolically, we may write

$$\bar{y} = y_e \pm \sigma/\sqrt{N} \approx y_e \pm \sigma_e/\sqrt{N}\,, \tag{A.3}$$

$$\sigma^2 \approx \sigma_e^2 (1 \pm \sqrt{2/N})\,. \tag{A.4}$$

Therefore, even with only $N = 160$, the variance is estimated with an accuracy of $\sim 10\%$. This shows that the fluctuations indicated in figs. 4, 7, 8, 10 are really meaningful. Note, however, that (A.3) applies for instance to average flow angle but not to the position of the peak of the $dN/d\cos\theta$ distribution, which is not a simple moment of the θ distribution.

Appendix B

FLOW AND MAXIMUM IN THE $dN/d\cos\theta$ DISTRIBUTION

Let us assume that the distribution (eq. (4.1)) depicted in fig. 7 is gaussian and has a maximum at some finite θ and for $\varphi = 0$. What is the condition that this distribution has to fulfil in order to generate a maximum at finite θ in the $dN/d\cos\theta$? To answer this question, we write the distribution (4.1) as

$$\frac{d^2N}{\rho\, d\rho\, d\varphi} = \frac{d^2N}{dx\, dy} = C \exp\left[-\frac{(x-x_0)^2+y^2}{2\sigma^2}\right]. \tag{B.1}$$

Here, x, y are the cartesian coordinates used in fig. 7 and C is a normalisation constant. We write

$$x = \rho\cos\varphi\,, \qquad y = \rho\sin\varphi\,, \tag{B.2}$$

and we recall that ρ is related to the flow angle by

$$\rho = \sin\theta\,.$$

Because of (4.2) we have

$$\frac{dN}{d\cos\theta} = C\cos\theta \exp\left(-\frac{\rho^2+x_0^2}{2\sigma^2}\right)\int_0^{2\pi} d\varphi \exp\left(\frac{\rho x_0}{2\sigma^2}\cos\varphi\right), \tag{B.3}$$

or

$$\frac{dN}{d(\cos\theta)} = 2\pi C\cos\theta \exp\left(-\frac{\sin^2\theta+x_0^2}{2\sigma^2}\right) I_0\left(\frac{x_0\sin\theta}{2\sigma^2}\right), \tag{B.4}$$

where I_0 is the usual modified Bessel function [44]). The latter increases when $\sin\theta$ increases, in contrast to the other factors which decrease. One can thus write down a condition to have a maximum at finite θ, by looking at the behaviour of expression (B.4) for small θ. One has

$$\frac{dN}{d(\cos\theta)} \alpha (1-\tfrac{1}{2}\sin^2\theta+\cdots)\times\left(1-\frac{\sin^2\theta}{2\sigma^2}+\cdots\right)\times\left(1+\frac{x_0^2}{16\sigma^4}\sin^2\theta+\cdots\right). \tag{B.5}$$

Therefore, the maximum will occur at $\theta = 0$, as long as

$$x_0 < 2\sigma\sqrt{2}(1+\sigma^2)\,. \tag{B.6}$$

This corroborates what we observed numerically for Ca+Ca, namely that a maximum at 0° can correspond to an intrinsic flow ($x_0 > 0$), provided the fluctuations are large enough.

References

1) H.-Å. Gustafsson *et al.*, Phys. Rev. Lett. **52** (1984) 1590
2) H.G. Ritter *et al.*, Proc. GSI Conf., Oct. 1984, GSI publication no. GSI-85-10 (1985) 67
3) H. Stöcker, J.A. Marhun and W. Greiner, Phys. Rev. Lett. **44** (1980) 725
4) H. Stöcker *et al.*, Phys. Rev. Lett. **47** (1981) 1807
5) H. Pirner, Phys. Rev. **C22** (1980) 1962
6) G. Bertsch and A.A. Amsden, Phys. Rev. **C18** (1978) 1293
7) J. Kapusta and D. Strottman, Phys. Lett. **106B** (1981) 33
8) R. Stock, Proc. 5th High Energy Heavy Ion Study, May 1981, LBL publication no. LBL-12652 (1981) 284
9) J. Cugnon, J. Knoll, C. Riedel and Y. Yariv, Phys. Lett. **109B** (1982) 167
10) A. Baden *et al.*, Nucl. Instr. Meth. **203** (1982) 189
11) Y. Yariv and Z. Fraenkel, Phys. Rev. **C20** (1979) 2227
12) Y. Yariv and Z. Fraenkel, Phys. Rev. **C24** (1981) 488
13) J. Cugnon, T. Mizutani and J. Vandermeulen, Nucl. Phys. **A352** (1981) 505
14) J. Cugnon and S.E. Koonin, Nucl. Phys. **A355** (1981) 477
15) J. Cugnon and D. L'Hôte, Nucl. Phys. **A397** (1983) 519
16) J. Cugnon and D. L'Hôte, Phys. Lett. **149B** (1984) 35
17) H. Stöcker, Proc. GSI Conf., Oct. 1984, GSI publication no. GSI-85-10 (1985) 197
18) J.J. Molitoris, H. Stöcker, H.-Å. Gustafsson, D. L'Hôte and J. Cugnon, to be published
19) J. Cugnon, D. Kinet and J. Vandermeulen, Nucl. Phys. **A379** (1982) 553
20) M. Gyulassy, K.A. Frankel and H. Stöcker, Phys. Lett. **110B** (1982) 185
21) D.E. Greiner *et al.*, Phys. Rev. Lett. **35** (1974) 152
22) A.S. Goldhaber, Phys. Lett. **53B** (1974) 306
23) H. Feshbach and K. Huang, Phys. Lett. **47B** (1973) 300
24) Y. Kitazoe *et al.*, Phys. Rev. Lett. **53** (1984) 2000
25) J. Cugnon and R. Lombard, Nucl. Phys. **A422** (1984) 635
26) P. Danielewicz and M. Gyulassy, Phys. Lett. **129B** (1983) 283
27) J. Cugnon, Cargèse Summer School, Sept. 1984 (Plenum, New York), to be published
28) J. Cugnon and D. L'Hôte, Proc. GSI Conf., Oct. 1984, GSI publication no. GSI-85-10 (1985) 253
29) K.G.R. Doss *et al.*, preprint GSI-85-4, Jan. 1985
30) H.-Å. Gustaffson, private communication
31) G. Bertsch, in Progress in particle and nuclear physics vol. 4, ed. D. Wilkinson (Pergamon, Oxford, 1980) p. 483
32) N.L. Balazs, B. Schürmann, K. Dietrich and L.P. Csernai, Nucl. Phys. **A424** (1984) 605
33) L.D. Landau and E.M. Lifshitz, Fluid mechanics (Pergamon, Oxford, 1975) ch. II
34) H.G. Ritter *et al.*, LBL-20086 (June 1985)
35) H.R. Jaqaman and A.Z. Mekjian, Phys. Rev. **C31** (1985) 146
36) J. Cugnon and D. L'Hôte, contribution to the Visby Conf., June 1985
37) P. Danielewicz and G. Odyniec, Phys. Lett. **B157** (1985) 146
38) G. Buchwald, G. Graebner, J. Theis, J. Marhun, W. Greiner and H. Stöcker, Phys. Rev. Lett. **52** (1984) 1590
39) M. Gyulassy, in Short distance phenomena in nuclear physics, ed. D.H. Boal and R.W. Woloshyn (Plenum, New York, 1983) p. 258
40) J.J. Molitoris, J.B. Hoffer, H. Kruse and H. Stöcker, Phys. Rev. Lett. **53** (1984) 899
41) G. Bertsch, H. Kruse and S. Das Gupta, Phys. Rev. **C29** (1984) 673
42) R. Malfliet, Phys. Rev. Lett. **53** (1984) 2386
43) J. Aichelin and G. Bertsch, Oak Ridge preprint (1985)
44) M. Abramowitz and I.A. Stegun, Handbook of mathematical functions (Dover, New York, 1970) ch. 9
45) M. Gyulassy, private communication